

Orthogonal Chirp Division Multiplexing for Power Line Sensing via Time-Domain Reflectometry

Lucas Giroto de Oliveira, *Student Member, IEEE*, Mateus de L. Filomeno,
and Moisés V. Ribeiro, *Senior Member, IEEE*

Abstract—In this study, a time-domain reflectometry (TDR) system based on a baseband version of the orthogonal chirp-division multiplexing (OCDM) scheme, which is relies on a modified discrete Fresnel transform (DFnT), is proposed for power line sensing. After a detailed description of the system model, a multiple access scheme that exploits the convolution theorem of the modified DFnT for enabling distributed reflectometric and transferometric sensing of the monitored power line. Considering typical European underground low-voltage and US overhead medium-voltage (MV) power distribution networks, range resolution and maximum unambiguous range for the measurements are assessed for the proposed scheme. Next, a comparison with multiple access schemes based on the Hermitian symmetric orthogonal frequency-division multiplexing (HS-OFDM) discussed in a previous work is performed considering a Brazilian MV overhead scenario, being the number of measurements obtained over time, as well as signal-to-interference-plus-noise ratio (SINR) used as performance metrics. The attained results show that the proposed multiple access scheme results in the same range resolution as the others. Also, the highest number of measurements over time is obtained by the proposed scheme, which produces orthogonality among signals transmitted by different power line modems (PLMs) neither and time nor frequency domains, but rather in the Fresnel domain. Meanwhile, although its yielded SINR values are fair among the PLMs consisting the distributed sensing system, the proposed scheme is slightly outperformed by the HS-OFDM based on code-division multiple access and by the HS-OFDM based on frequency-division multiple access at some PLMs.

Index Terms—Time-domain reflectometry, orthogonal chirp-division multiplexing, multiple access, power line communication.

I. INTRODUCTION

In the context of modern power line diagnosis, the use of higher frequencies than the mains has been widely considered in recently proposed techniques. A main reason for that is the higher amount of information that can be extracted from the monitored network by monitoring harmonic voltages and currents [1], [2], or even traveling waves [3] in a wider frequency band, allowing more efficient sensing of anomalies such as high impedance fault (HIF) and cable degradation.

Manuscript received month day, year; revised month day, year. This study was financed in part by the Coordenação de Aperfeiçoamento de Pessoal de Nível Superior - Brasil (CAPES) - Finance Code 001, Copel Distribuição LTD - PD 2866-0420/2015, CNPq, FAPEMIG, INERGE and Smarti9 LTD.

Lucas Giroto de Oliveira and Mateus de L. Filomeno are with the Electrical Engineering Department, Federal University of Juiz de Fora (UFJF), Juiz de Fora, Brazil (e-mail: lgiroto@ieee.org, mateus.lima@engenharia.ufjf.br).

Moisés V. Ribeiro is with the Electrical Engineering Department, Federal University of Juiz de Fora (UFJF), Juiz de Fora, Brazil, and Smarti9 Ltd, Brazil (e-mail: mribeiro@ieee.org).

For enabling travelling wave-based approaches, the use of power line communication (PLC) technology is an interesting alternative that has been recently considered [4]. Topics ranging from adjustments to power line modems (PLMs) for enabling network sensing [5] to machine learning-aided power line monitoring [6] have been investigated. Also, reflectometric [7] and transferometric [8] sensing of power lines have been given attention.

In this context, time-domain reflectometry (TDR) techniques such as multicarrier time-domain reflectometry (MCTDR) [9]–[11] and its orthogonal frequency-division multiplexing (OFDM)-based version orthogonal multitone time-domain reflectometry (OMTDR) [12] allow effective digital signal processing while allowing simplified spectrum managing for complying to electromagnetic compatibility (EMC) constraints. Originally considered for wired networks scenarios such as aircraft, a variation of the latter has been studied in [13] considering a channel estimation procedure instead of the classical pulse compression.

For enabling more efficient sensing, an efficient solution is to perform distributed reflectometric and transferometric sensing of the monitored network. Aiming such purpose, research efforts have already been done for multicarrier-based TDR systems [14]. Also, multiple access schemes based on time-division multiple access (TDMA), frequency-division multiple access (FDMA), and code-division multiple access (CDMA), have been studied for TDR systems based on the baseband version of OFDM, i.e. Hermitian symmetric OFDM (HS-OFDM), in the context of power distribution network sensing [13].

Recently, orthogonal chirp-division multiplexing (OCDM), which is a multicarrier scheme based on the discrete Fresnel transform (DFnT), has been proposed for wireless systems [15]. Such scheme has shown robustness to multipath propagation, being an interesting alternative for digital data communication. Furthermore, four modified versions of DFnT that allow the extension of such scheme for baseband data transmission in PLC systems have been proposed [16]. One of these four versions, named Type III OCDM in [16], adds Hermitian symmetry to the DFnT matrix in order to produce a real-valued transmit vector in the discrete-time domain demanding low computational complexity. Considering the modified DFnT of the Type III OCDM from [16], this study describes an OCDM-based TDR system for power line sensing. Based on the convolution theorem of the DFnT, which also holds for the modified DFnT, a multiple access scheme is then introduced for the OCDM-based TDR system. Finally, the proposed

multiple access scheme is compared with HS-OFDM-based TDMA, FDMA, and CDMA schemes in order to assess its effectiveness.

Given this background, the contributions of this study are as follows.

- 1) Modelling of an OCDM-based TDR system for power line sensing considering the single PLM case. In the context of this formulation, a multiple access scheme exploiting the convolution theorem of the modified DFNT for distributed power line sensing is introduced.
- 2) Performance assessment and comparison of the proposed OCDM-based multiple access scheme for power line sensing via TDR with the HS-OFDM-based TDMA, FDMA, and CDMA multiple access schemes.

Based on the attained results, our major findings are as follows.

- 1) The OCDM-based multiple access scheme performs equally to the HS-OFDM-based counterparts in terms of range resolution. Regarding maximum unambiguous range, it is more affected by the measurement window length in the proposed scheme and the HS-OFDM/FDMA scheme than in the remaining schemes respectively due to the subchirp and subcarrier allocation among the PLMs. The considered scenarios for assessing range resolution and maximum unambiguous range values attained by the proposed scheme are typical European underground low-voltage and US overhead medium-voltage power distribution networks, while the system parameters are based on narrowband (NB)-PLC standards.
- 2) Both the proposed OCDM-based and the HS-OFDM/FDMA multiple access schemes yield much higher number of reflectograms and transferograms than the remaining considered schemes over time. They are, therefore, more appropriate for continuously performing distributed sensing of power lines and consequently sensible to intermittent faults, being the latter feature common to the HS-OFDM/CDMA scheme in certain cases [14].
- 3) Considering a Brazilian overhead medium voltage (MV) scenario and maintaining the system parametrization, equal performance to the HS-OFDM/TDMA scheme in terms of signal-to-interference-plus-noise ratio (SINR) is attained by the proposed OCDM-based multiple access scheme. Meanwhile, the SINR is increased or decreased at different PLMs in the HS-OFDM/FDMA scheme due to the combination of the subcarrier hopping among PLMs and exponentially decaying power spectral density (PSD). Finally, the best SINR performance is attained by the HS-OFDM/CDMA scheme, which is a consequence of the noise averaging at the decoding process [13], [14].

The remainder of this paper is organized as follows. The OCDM-based TDR system for sensing of a power distribution network is described in Section II considering the single PLM case. Next, Section III discusses range resolution and maximum unambiguous range aspects of the considered TDR system and introduces a novel multiple access scheme based

on OCDM. Numerical results and discussions are presented in Section IV for evaluating the proposed multiple access scheme with HS-OFDM-based counterparts, and concluding remarks are placed in Section V. Finally, the convolution theorem of the modified DFNT is demonstrated in the Appendix.

Notation

Throughout the paper, $\delta(t)$ and $\delta[k]$ are respectively the Dirac and Kronecker delta functions; $(\cdot)^\dagger$ indicates the Hermitian transpose operator; $\mathbb{E}\{\cdot\}$ represents the expectation operator; $\mathbf{diag}\{\cdot\}$ converts the argument vector into a diagonal matrix; \mathbf{I}_M is a M -size identity matrix; the M -size discrete Fourier transform (DFT) matrix is denoted by \mathbf{W}_M ; and Φ_M is the M -size modified DFNT matrix, which is the baseband version of the DFNT matrix.

II. SYSTEM MODEL

Let a baseband TDR system be consisted by a full-duplex PLM connected to a power distribution network, which, at a single given point, injects signals and captures reflections that travel at a phase velocity v_p . Assuming that the injection and subsequent capture of reflections of signals takes place within a coherence time T_c , in which variations in loads or any other element of the network are irrelevant, one can consider the power distribution network as a linear time-invariant (LTI) system. The reflections captured by the PLM from such power distribution network, which are raised by impedance discontinuities along the path traveled by the injected signal, are therefore the output of a reflection channel with impulse response expressed as

$$h_\Gamma(t) = \sum_{i=0}^{N_\Gamma-1} \alpha_i \delta(t - T_i), \quad (1)$$

where N_Γ is the number of impedance discontinuities experienced by the injected signal, while α_i and T_i are respectively the attenuation factor and the arrival time at the receiver side of the PLM associated with the reflection raised by the i^{th} impedance discontinuity, $i \in \{0, \dots, N_\Gamma - 1\}$.

A reflectometric sensing of the power distribution network, which consists of an analysis of the reflections raised by the impedance discontinuities along its length, can be used for applications such as topology inference and fault detection and location. Such task can be performed by a TDR system which is capable of obtaining estimates of the reflection channel impulse response, named *reflectograms*. In this study, it is assumed that such TDR system is based on a baseband OCDM scheme that is band-limited to a bandwidth B and has sampling frequency $F_s = 2B$.

The considered OCDM-based TDR system is depicted in Fig. 1, starting with a real discrete-Fresnel domain vector $\dot{\mathbf{x}} = [\dot{x}_0, \dot{x}_1, \dots, \dot{x}_{2N-1}]^T$, such that $\dot{\mathbf{x}} \in \mathbb{R}^{2N \times 1}$. This vector is inputted to the function $\mathcal{P}(\cdot)$ that represents, in a condensed form, the twofold digital processing performed at the transmitter side. The first processing stage performed by $\mathcal{P}(\cdot)$ is a modified inverse discrete Fresnel transform (IDFNT) on $\dot{\mathbf{x}}$, which generates the $2N$ -length discrete-time domain

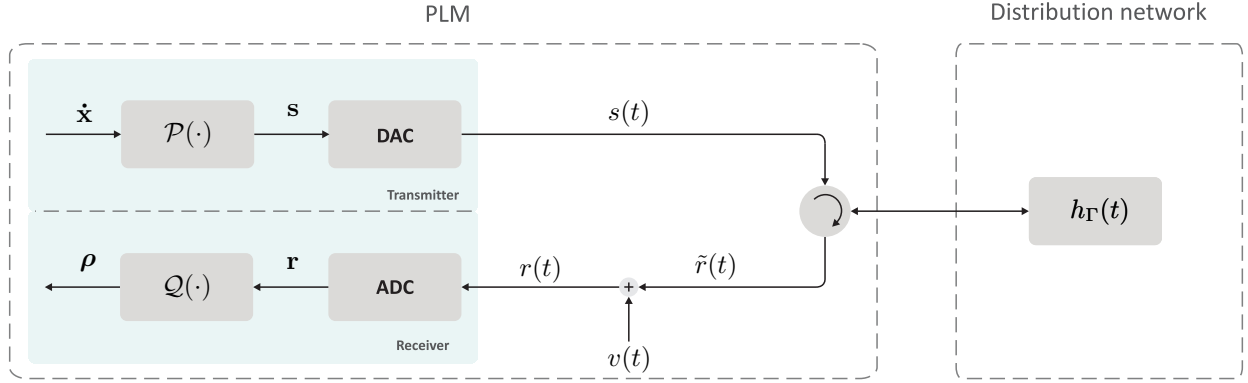


Fig. 1: OCDM-based baseband TDR system over a distribution network.

vector $\mathbf{x} = \Phi_{2N}^\dagger \hat{\mathbf{x}}$, $\mathbf{x} \in \mathbb{R}^{2N \times 1}$. Finally, an L_{cp} -length cyclic prefix is appended to \mathbf{x} , resulting in the vector $\mathbf{s} \in \mathbb{R}^{(2N+L_{cp}) \times 1}$. Considering that the reflection channel impulse response has an $L_{h,\Gamma}$ -length discrete-time domain representation $\mathbf{h}_\Gamma = [h_{\Gamma,0}, h_{\Gamma,1}, \dots, h_{\Gamma,L_{h,\Gamma}-1}]^T$, $\mathbf{h}_\Gamma \in \mathbb{R}^{L_{h,\Gamma} \times 1}$, no intersymbol interference (ISI) is experienced if the constraint $L_{cp} \leq L_{h,\Gamma}$ is satisfied.

Back to Fig. 1, the discrete-time vector \mathbf{s} undergoes an digital-to-analog conversion, being converted into the continuous-time signal $s(t)$ that is inputted to the reflection channel of impulse response $h_\Gamma(t)$. It is worth highlighting that, in order for the LTI assumption of the reflection channel to hold, the duration of $s(t)$, i.e., the OCDM symbol in the continuous-time domain, $T_{\text{symbol}} = (2N + L_{cp})T_s$ must satisfy the constraint $T_{\text{symbol}} \ll T_c$. The first term of the previous expression accounts for the number of samples of the discrete-time vector \mathbf{s} , while $T_s = 1/F_s$ is the sampling period. The resulting signal from the convolution between the transmit signal and the channel is $\tilde{r}(t) = s(t) \star h_\Gamma(t)$. To this signal is added the noise $v(t)$, which is a zero-mean wide-sense stationary (WSS) random process, resulting in the received signal $r(t) = s(t) \star h_\Gamma(t) + v(t)$. Note that, due to the noise presence, $r(t)$ is also a WSS random process.

At the receiver side, the signal $r(t)$ passes through an analog-to-digital converter, originating the discrete-time domain vector $\mathbf{r} \in \mathbb{R}^{(2N+L_{cp}) \times 1}$. Next, \mathbf{r} is inputted to the function $\mathcal{Q}(\cdot)$, which synthesizes the digital processing at the receiver side of the OCDM-based TDR system. The performed processing by this function starts with cyclic prefix removal from \mathbf{r} , which originates the discrete-time domain vector $\mathbf{y} \in \mathbb{R}^{2N \times 1}$ expressed as

$$\mathbf{y} = \mathbf{H}_\Gamma \mathbf{x} + \mathbf{v}, \quad (2)$$

where $\mathbf{H}_\Gamma \in \mathbb{R}^{2N \times 2N}$ is a circulant matrix associated with a zero-padded version of \mathbf{h}_Γ , and $\mathbf{v} \in \mathbb{R}^{2N \times 1}$ is a $2N$ -length discrete-time domain window of the additive noise $v(t)$.

The next processing stage of $\mathcal{Q}(\cdot)$ consists of performing a modified DFNT on \mathbf{y} , originating the discrete-Fresnel domain vector $\hat{\mathbf{y}} \in \mathbb{R}^{2N \times 1}$. As the convolution theorem of the DFNT also holds for the modified DFNT, which is demonstrated in the Appendix, $\hat{\mathbf{y}}$ can be equivalently expressed as

$$\hat{\mathbf{y}} = \mathbf{H}_\Gamma \hat{\mathbf{x}} + \hat{\mathbf{v}}, \quad (3)$$

being $\hat{\mathbf{v}} = [\hat{v}_0, \hat{v}_1, \dots, \hat{v}_{2N-1}]^T$, $\hat{\mathbf{v}} \in \mathbb{R}^{2N \times 1}$, a $2N$ -length discrete-Fresnel domain window of the additive noise $v(t)$.

The processing performed by $\mathcal{Q}(\cdot)$ is completed with the obtaining of an L_ρ -length reflectogram from $\hat{\mathbf{y}}$, denoted in the discrete-time domain as $\boldsymbol{\rho} \in \mathbb{R}^{L_\rho \times 1}$, $L_\rho \geq L_{h,\Gamma}$. Besides ensuring high signal-to-noise ratio (SNR) in order for noise effect to be negligible, a proper reflectogram must have the influence of the transmit vector $\hat{\mathbf{x}}$ on it minimized or eliminated so that it is a good estimate of the reflection channel impulse response \mathbf{h}_Γ . In this study, this is accomplished by simply designing a proper $\hat{\mathbf{x}}$ so that $\boldsymbol{\rho}$ is directly obtained from $\hat{\mathbf{y}}$ with no additional processing. Also, for covering cases where multiple PLMs are to perform network sensing simultaneously, this design must also enable orthogonal multiple access among the PLMs. A discussion on the design of $\hat{\mathbf{x}}$ is presented in Section III.

Once $\boldsymbol{\rho}$ has been obtained, its analog counterpart $\rho(t)$ can be yielded in order to reduce the temporal granularity and, as a consequence, the spatial granularity of the reflectogram and the impedance discontinuity location accuracy. As discussed in [13], an interesting approach for the considered system would be sinc interpolation in the time domain by a reconstruction filter [17] as the reflectogram is directly obtained in the discrete-time domain.

III. DISTRIBUTED POWER LINE SENSING

As discussed in Section II, for obtaining a proper reflectogram from the discrete-Fresnel domain vector $\hat{\mathbf{y}}$, the influence of the discrete-Fresnel domain transmit vector $\hat{\mathbf{x}}$ on it as expressed in (3) must be minimized or ideally removed. Considering that a single PLM performs sensing of the power distribution network, a transmit vector $\hat{\mathbf{x}}$ constituted of pilots spaced by L_ρ samples in the discrete Fresnel domain can be used [18], [19]. Thus, the k^{th} element of $\hat{\mathbf{x}}$ will be given by

$$\hat{x}_k = \sum_{u=0}^{2N/L_\rho-1} \delta[k - uL_\rho], \quad (4)$$

in which $k \in \{0, \dots, 2N-1\}$. Based on the convolution theorem of the modified DFNT, the k^{th} element of the resulting

discrete-Fresnel domain received vector $\hat{\mathbf{y}}$ can be expressed as

$$\hat{y}_k = \left(\sum_{u=0}^{2N/L_\rho-1} h_{\Gamma, k-uL_\rho} \right) + \hat{v}_k, \quad (5)$$

Note that $h_{\Gamma, k-uL_\rho} = 0$ for $k - uL_\rho < 0$ and $k - uL_\rho > L_{h,\Gamma} - 1$, as $h_{\Gamma, k}$ is only defined for $k \in \{0, \dots, L_{h,\Gamma} - 1\}$. As a consequence, $\hat{\mathbf{y}}$ will be constituted of concatenated estimates of the reflection channel impulse response impaired by additive noise, which will not cause mutual interference on each other if the spacing between consecutive pilots is equal to or longer than the length of \mathbf{h}_Γ , i.e. $L_\rho \geq L_{h,\Gamma}$. Finally, $2N/L_\rho$ unbiased discrete-time domain reflectograms are obtained by dividing the discrete-Fresnel domain vector $\hat{\mathbf{y}}$ into L_ρ -length windows. Such channel estimation is therefore equivalent to an ideal pulse compression procedure, whose capability of distinguishing reflections caused by close impedance discontinuities, i.e. range resolution, is given by [7], [13]

$$\Delta d = \frac{v_p}{4B}. \quad (6)$$

Additionally, the peak-to-sidelobe level ratio (PSLR) and integrated-sidelobe level ratio (ISLR) levels of each obtained estimate will only depend upon the occupied frequency bandwidth B in the baseband by the TDR system as described in [13].

In the proposed OCDM-based TDR system, the maximum unambiguous range is limited by both the measurement window length L_ρ and the cyclic prefix length L_{cp} . As previously discussed, L_ρ must be set so that there is no mutual interference among measurement windows. L_{cp} , in its turn, must be long enough so that no ISI is experienced. Based on the discussion carried out in [13], the maximum unambiguous range for reflectograms is

$$d_{\max,R} = \frac{v_p T_s}{2} \min\{L_\rho, L_{cp}\}. \quad (7)$$

For transferograms, the maximum unambiguous range is

$$d_{\max,T} = v_p T_s \min\{L_\rho, L_{cp}\}, \quad (8)$$

which is twice the value assumed by $d_{\max,r}$, in which the round trip time for the transmitted travelling waves is considered.

Moving to the case where N_{PLM} PLMs perform sensing of a single power distribution network simultaneously, an efficient multiple access strategy must be adopted. In the case of HS-OFDM-based TDR systems, TDMA, FDMA, and CDMA schemes have been discussed in a previous study [13]. For the case of the OCDM-based TDR system considered in this study, the orthogonality among the signals associated with the multiple PLMs is ensured by a proper subchirp allocation among them.

The proposed subchirp allocation scheme for enabling multiple access among PLMs performing unbiased power line sensing is shown in Fig. 2. In this figure, the subchirp pilot of index $k = uL_\rho$ of the $2N$ -length discrete-Fresnel domain transmit vector $\hat{\mathbf{x}}$ is active for the u^{th} PLM, $u \in \{0, \dots, N_{PLM} - 1\}$. For the sake of fairness, the distance

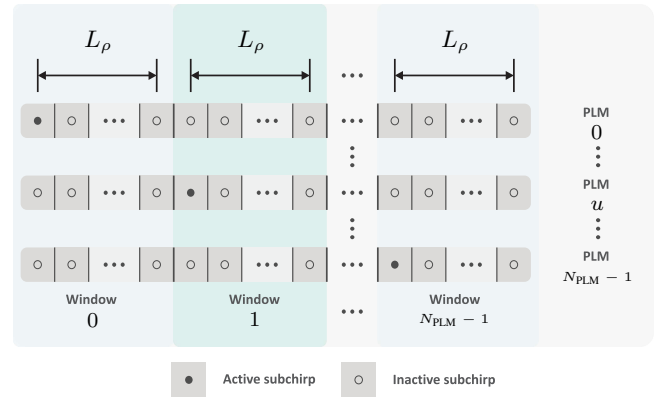


Fig. 2: Subchirp allocation among the PLMs.

between the sample associated with the active pilot of the u^{th} PLM and sample associated with the active pilot of the $(u+1)^{th}$ PLM is set to $L_\rho = 2N/N_{PLM}$.

At the receiver side, the vector $\hat{\mathbf{y}}$ at the u^{th} PLM will be composed by N_{PLM} measurement windows. The u^{th} measurement window starts at the subchirp $k = uL_\rho$ and ends at the subchirp $k = uL_\rho + L_\rho - 1$ of $\hat{\mathbf{y}}$ and it is a reflectogram at the u^{th} PLM and a transferogram at the remaining PLMs. In order to perform effective network sensing, data fusion techniques can be applied on the obtained measurement windows [8].

In order to avoid interference among measurement windows, the spacing among pilots must satisfy the constraint $L_\rho = 2N/N_{PLM} \geq L_{h,\max}$, or alternatively

$$2N \geq N_{PLM} L_{h,\max}. \quad (9)$$

For this constraint, $L_{h,\max}$ is defined as

$$L_{h,\max} \triangleq \max_{ij} \{L_{h,ij}\}, \quad (10)$$

where $L_{h,ij}$ is the length of the channel impulse response $\mathbf{h}_{ij} \in \mathbb{R}^{L_{h,ij} \times 1}$ for a signal injected by the j^{th} PLM into the network and received by the i^{th} PLM, with $i \in \{0, \dots, N_{PLM} - 1\}$ and $j \in \{0, \dots, N_{PLM} - 1\}$. Altogether, there are N_{PLM}^2 channel impulse responses \mathbf{h}_{ij} , with a total of N_{PLM} reflectograms (\mathbf{h}_{ij} , $i = j$) and $N_{PLM}(N_{PLM} - 1)$ transferograms (\mathbf{h}_{ij} , $i \neq j$).

The proposed multiple access scheme and system parametrization result in the obtaining of a number

$$N_\rho = \frac{1}{T_{\text{symp}}} \quad (11)$$

reflectograms per PLM per second. Additionally, a number is

$$N_\tau = \frac{N_{PLM} - 1}{T_{\text{symp}}} \quad (12)$$

of transferograms are obtained per PLM per second, resulting in a total number of $N_{\text{meas}} = N_\rho + N_\tau = N_{PLM}/T_{\text{symp}}$ measurements per PLM per second.

IV. NUMERICAL ANALYSIS

In order to validate the carried out discussion, numerical results are presented and discussed in this section. Given

this context, Subsection IV-A presents range resolution and maximum unambiguous range values for the OCDM-based TDR system considering typical system parametrizations for NB-PLC systems, while Subsection IV-B carries out a comparative analysis of the proposed OCDM-based distributed TDR system with the HS-OFDM-based counterpart with TDMA, FDMA, and CDMA multiple access schemes described in a previous study [13].

A. Range resolution and maximum unambiguous range

For performing proper sensing of a power distribution network, it is paramount to have awareness of the TDR system limitations resulting from its parametrization. In this context, an European underground low-voltage power distribution network and an US overhead medium-voltage power distribution network in a rural area are considered for range resolution and maximum unambiguous range analysis. For the low-voltage scenario, it is considered a power supply cable NAYY150SE with resistance R' , inductance L' , conductance G' , and capacitance C' per unit length calculated as in [20], whereas for the medium-voltage cable, the power supply cable with distributed parameters listed in [21] is adopted. Based on these parameters, the phase velocity is calculated by $v_p = 1/\sqrt{L'C'}$ [22], resulting in $v_p = 1.50 \times 10^8$ for the considered low voltage (LV) cable, and $v_p = 2.56 \times 10^8$ for the considered MV cable.

Fig. 3 shows the range resolution Δd as a function of the occupied frequency bandwidth B for the considered LV and MV scenarios. The achieved Δd values range from tens of thousands of kilometers for low B values to a few meters for higher B values, with a ratio of 1.71 between the resolution in the MV and LV and scenarios due to their different phase velocity. The presented results indicate that B values in the NB-PLC frequency range, i.e., $B < 500$ kHz, result in fair range resolution values, i.e., $\Delta d \geq 75$ m, and therefore a fair capability of resolving close impedance discontinuities for typical distances covered by PLC signaling in LV and MV power distribution networks, which are about 1 km in MV scenarios and shorter in LV scenarios [5], [23]. Given this result, the parameters listed in Table I, which are based on typical NB-PLC standards [21], are adopted for the results presented henceforth.

Next, Fig. 4 shows the maximum unambiguous ranges $d_{\max,\rho}$ and $d_{\max,\tau}$ as functions of the cyclic prefix length L_{cp} for different numbers of PLMs N_{PLM} in the considered LV and MV scenarios. One observes $d_{\max,\rho} = 1.87$ km and $d_{\max,\tau} = 3.75$ km in the LV scenario and $d_{\max,\rho} = 3.21$ km and $d_{\max,\tau} = 6.41$ km in the MV scenario for $N_{PLM} \leq 4$ if $L_{cp} = 30$. For $N_{PLM} > 4$, the measurement window length L_ρ becomes shorter than L_{cp} , reducing the maximum unambiguous ranges according to the relation described in (7) and (8). In the case where $L_{cp} = 52$ is adopted, a similar behavior is observed. For $N_{PLM} \leq 8$, maximum unambiguous range values of $d_{\max,\rho} = 3.25$ km and $d_{\max,\tau} = 6.50$ km are observed in the LV scenario, while the values $d_{\max,\rho} = 5.56$ km and $d_{\max,\tau} = 11.11$ km are observed in the MV scenario. As in the previous case, an increase in N_{PLM} results in

TABLE I: Adopted system parameters.

System parameters		
Frequency range (kHz)	0 – 500	
Frequency bandwidth B (kHz)	500	
Sampling frequency F_s (MHz)	1	
OCDM symbol length $2N$	256	
Cyclic prefix length L_{cp}	Standard	30
	Long	52

considerable reduction of the maximum unambiguous range values.

B. Comparison with multiple access schemes for HS-OFDM-based TDR systems

The next aspect of the numerical analysis is a comparison of the proposed OCDM-based multiple access scheme for distributed power line sensing with the TDMA, FDMA, and CDMA multiple access schemes described in [13] for HS-OFDM-based TDR systems. For this purpose, the system parameters listed in I are maintained and binary phase-shift keying (BPSK) modulation is adopted. Additionally, a multiconductor transmission line (MTL)-based model [22], [24] of a real MV power distribution network section in

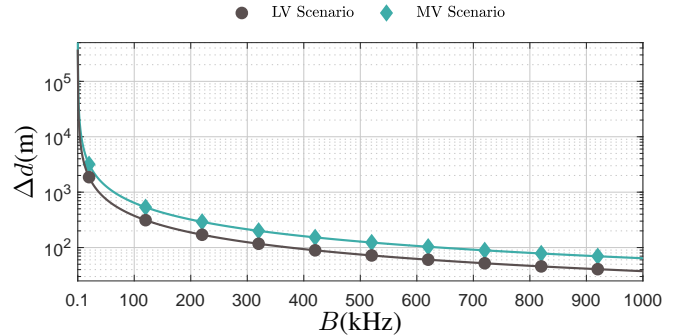


Fig. 3: Range resolution Δd in meters as a function of the occupied frequency bandwidth B in the considered LV and MV scenarios [13].

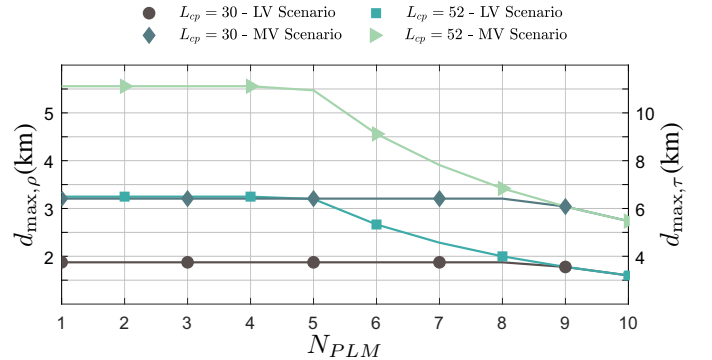


Fig. 4: Maximum unambiguous range for reflectograms $d_{\max,\rho}$ and transferograms $d_{\max,\tau}$ as functions of the number of PLMs N_{PLM} .

the city of Curitiba, Brazil, described in [13] and depicted in Fig. 5 is considered. Finally, the adopted additive noise model is the one reported in [25], [26], whose one-sided PSD in the continuous-frequency domain is $S_V(f) = -93 + 52.98e^{-0.0032f/10^3}$ dBm/Hz.

Given the considered scenario, the number of obtained reflectograms over time N_ρ for the considered multiple access schemes as a function of N_{PLM} is shown in Fig. 6a for $L_{cp} = 30$ and in Fig. 6b for $L_{cp} = 52$. While TDMA and CDMA for HS-OFDM-based TDR systems yield a decreasing number of reflectograms along with the number of PLMs due to time multiplexing and HS-OFDM symbol spreading, respectively, the use of the proposed OCDM-based multiple access scheme, as well as of the HS-OFDM/FDMA, results in a higher and constant number of reflectograms regardless of the number of PLMs.

The attained number of transferograms over time N_τ is shown Fig. 7a for $L_{cp} = 30$ and in Fig. 7b for $L_{cp} = 52$. As expected according to (12), no transferogram is obtained for $N_{PLM} = 1$. The presented results also show rapidly increasing N_τ values along with N_{PLM} for the proposed OCDM-based scheme and HS-OFDM/FDMA, while HS-OFDM/TDMA and HS-OFDM/CDMA yield slower increasing N_τ along with N_{PLM} . The reasons for such behavior are the same as in the case of reflectograms.

The last stage of the numerical analysis of this study is a performance comparison among the proposed OCDM-based multiple access scheme and the ones discussed for HS-OFDM-based TDR systems in terms of the associated SINR to the obtained measurements. For the sake of simplicity, only reflectograms are considered. Also, an one-sided PSD of -40 dBm/Hz for the transmit signal has been adopted. Such assumption results in total transmission power values of 20 dBm for the proposed OCDM-based multiple access scheme as well as the HS-OFDM/TDMA and HS-OFDM/CDMA schemes, while the total transmission power for the HS-OFDM/FDMA scheme is 13.98 dBm as not all subcarrier are active at each PLM. Of all the considered schemes, only the HS-OFDM/CDMA presents mutual interference among the PLMs as described in [13], being the SINR for the OCDM-based scheme as well as for HS-OFDM/TDMA and HS-OFDM/FDMA equal to their associated SNR.

The resulting SINR for the four PLMs in the considered

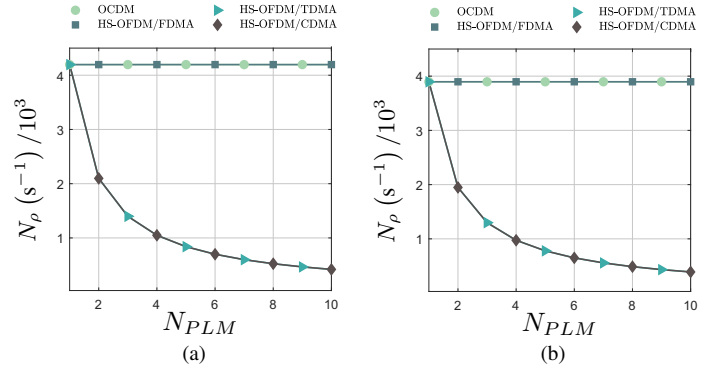


Fig. 6: Number of obtained reflectograms N_ρ as a function of the number of PLMs N_{PLM} for (a) $L_{cp} = 30$, and (b) $L_{cp} = 52$.

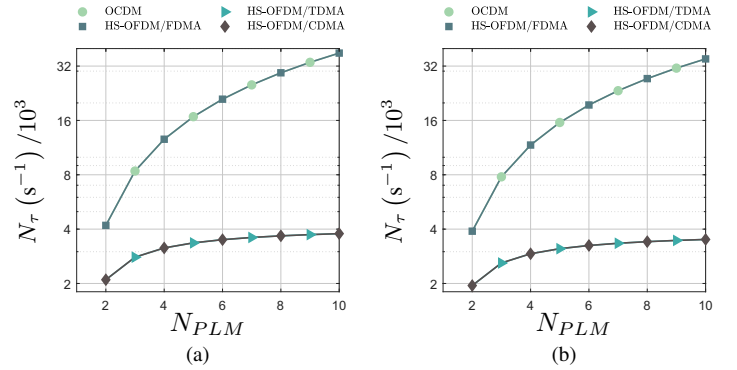


Fig. 7: Number of obtained transferograms N_τ as a function of the number of PLMs N_{PLM} for (a) $L_{cp} = 30$, and (b) $L_{cp} = 52$.

multiple access schemes are presented in Table II. Due to the exponentially decreasing additive noise PSD and the subcarrier hopping, the HS-OFDM/FDMA yields higher SINR values at PLMs to which higher-frequency subcarriers are allocated. In the HS-OFDM/CDMA scheme, the higher SINR values, which unlike the FDMA case are fair among the PLM, are explained by the averaging process in the decoding procedure [13], [14]. Finally, HS-OFDM/TDMA and the proposed OCDM-

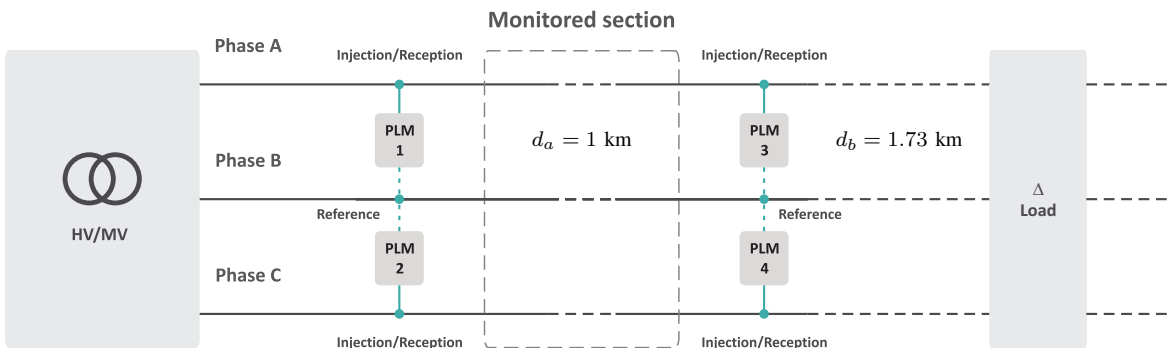


Fig. 5: Considered MV distribution network section [13].

TABLE II: SINR of the reflectograms at the four PLMs for the considered multiple access schemes.

SINR (dB)				
PLM index u	1	2	3	4
OCDM	14.85dB	14.85dB	14.85dB	14.85dB
HS-OFDM/TDMA	14.85dB	14.85dB	14.85dB	14.85dB
HS-OFDM/FDMA	13.83dB	14.54dB	15.28dB	16.04dB
HS-OFDM/CDMA	17.87dB	17.87dB	17.87dB	17.87dB

based multiple access scheme yield fair SINR values without any increase or decrease, and at a same level for all PLMs. This happens due to two factors, which are: i) unlike the HS-OFDM/FDMA case, all spectral content in the frequency bandwidth B is contained in the reflectogram; and ii) there is no averaging process reducing the effective noise power and therefore increasing the SINR as in the HS-OFDM/CDMA scheme.

V. CONCLUSION

In this study, a novel multiple access scheme for OCDM-based TDR systems performing distributed power line sensing has been proposed. First, an OCDM-based TDR system considering a single PLM has been described, being its range resolution and maximum unambiguous range aspects for both reflectograms and transferograms addressed. Next, the proposed multiple access scheme has been introduced and its implications on system parametrization and performance have been discussed. Finally, a numerical analysis has been carried out to support the discussion carried out throughout the paper.

The attained results have illustrated the dependence of the range resolution on the occupied frequency bandwidth as well as the effect of measurement window length and cyclic prefix length on the maximum unambiguous range, both considering typical European underground LV and US overhead MV scenarios. A comparison with a previous work [13] shows that such effects are equally present in the HS-OFDM-based TDR systems based on TDMA, FDMA, and CDMA multiple access schemes, being the range resolution equal among all schemes and the maximum unambiguous range the most influenced by the measurement window length in the proposed OCDM-based and HS-OFDM/FDMA schemes respectively due to the subchirp and subcarrier allocation among the PLMs. On the other hand, these schemes yield a much higher number of reflectograms and transferograms over time than the HS-OFDM/TDMA and HS-OFDM/CDMA schemes, which are respectively impaired by their time multiplexing and spreading processes. The proposed OCDM-based multiple access scheme is therefore appropriate for continuously performing distributed sensing of a power line.

Finally, the results obtained considering the described Brazilian overhead MV scenario have shown that the proposed scheme performs equally to the HS-OFDM/TDMA scheme in terms of SINR. In comparison to the HS-OFDM/FDMA scheme, the OCDM-based scheme performs better for 2 PLM and worse for the other 2 PLM due to the combined effect

of subcarrier hopping and exponentially decaying PSD that increases or decreases the SINR for different PLMs in the former scheme. The best performance, however, is still attained by the HS-OFDM/CDMA scheme due to its averaging process that reduces the effective additive noise power.

APPENDIX

To introduce the modified DFNT, the diagonal matrix $\mathbf{\Gamma}_{2N} = \text{diag}\{\Gamma_{0,0}, \Gamma_{1,1}, \dots, \Gamma_{2N-1,2N-1}\}$ is defined. The elements $\Gamma_{k,k}$, $k = 0, \dots, 2N-1$ of $\mathbf{\Gamma}_{2N} \in \mathbb{C}^{2N \times 2N}$ are defined as

$$\Gamma_{k,k} \triangleq \begin{cases} e^{-j\pi/2N}(k^2), & k \leq N \\ e^{j\pi/2N}(k^2), & k > N \end{cases}. \quad (13)$$

It clearly holds that $\mathbf{\Gamma}_{2N}\mathbf{\Gamma}_{2N}^\dagger = \mathbf{I}_{2N}$. The diagonal matrix $\mathbf{\Gamma}_{2N}$ inputs are the eigenvalues of a circulant matrix $\mathbf{\Phi}_{2N} \in \mathbb{R}^{2N \times 2N}$ such that

$$\mathbf{F}_{2N}\mathbf{\Phi}_{2N}\mathbf{F}_{2N}^\dagger = \mathbf{\Gamma}_{2N}, \quad (14)$$

where $\mathbf{F}_{2N} = (1/\sqrt{2N})\mathbf{W}_{2N}$. The real circulant matrix $\mathbf{\Phi}_{2N}$ from (14) is the modified DFNT matrix used for transforming a discrete-time domain vector $\mathbf{c} \in \mathbb{R}^{2N \times 2N}$ into the discrete-Fresnel domain vector $\hat{\mathbf{c}} \in \mathbb{R}^{2N \times 2N}$ via the operation

$$\hat{\mathbf{c}} = \mathbf{\Phi}_{2N}\mathbf{c}, \quad (15)$$

The inverse DFNT is achieved therefore by

$$\mathbf{c} = \mathbf{\Phi}_{2N}^\dagger\hat{\mathbf{c}}. \quad (16)$$

The convolution theorem, as well as the unitary and the similarity transformation properties of the modified DFNT, on which the former is based, are demonstrated as follows.

Unitary property of the modified DFNT

For the circulant modified DFNT matrix $\mathbf{\Phi}_{2N}$ from (14), it holds the unitary property, i.e.,

$$\begin{aligned} \mathbf{\Phi}_{2N}^\dagger\mathbf{\Phi}_{2N} &= (\mathbf{F}_{2N}^\dagger\mathbf{\Gamma}_{2N}\mathbf{F}_{2N})(\mathbf{F}_{2N}^\dagger\mathbf{\Gamma}_{2N}^\dagger\mathbf{F}_{2N}) \\ &= \mathbf{I}_{2N}. \end{aligned} \quad (17)$$

Due to the Hermitian symmetry of $\mathbf{\Gamma}_{2N}$ observed in (13), one has that $\mathbf{\Phi}_{2N} \in \mathbb{R}^{2N \times 2N}$, which enables baseband applications for the presented DFNT matrix.

Similarity transformation of the modified DFNT

For the given circulant DFNT matrix, it also holds the similarity transformation expressed as

$$\mathbf{\Phi}_{2N}\mathbf{Z}\mathbf{\Phi}_{2N}^\dagger = \mathbf{Z}, \quad (18)$$

in which $\mathbf{Z} \in \mathbb{R}^{2N \times 2N}$ is a circulant matrix. The proof for (19) starts by rearranging the expression as

$$\mathbf{\Phi}_{2N}\mathbf{Z}\mathbf{\Phi}_{2N}^\dagger = (\mathbf{F}_{2N}^\dagger\mathbf{\Gamma}_{2N}^\dagger\mathbf{F}_{2N})\mathbf{Z}(\mathbf{F}_{2N}^\dagger\mathbf{\Gamma}_{2N}\mathbf{F}_{2N}). \quad (19)$$

We next write

$$\mathbf{\Phi}_{2N}\mathbf{Z}\mathbf{\Phi}_{2N}^\dagger = \mathbf{F}_{2N}^\dagger\mathbf{\Gamma}_{2N}^\dagger\mathbf{\Gamma}_Z\mathbf{\Gamma}_{2N}\mathbf{F}_{2N}, \quad (20)$$

in which $\Gamma_Z = \mathbf{F}_{2N} \mathbf{Z} \mathbf{F}_{2N}^\dagger$ is a diagonal matrix whose inputs are the eigenvalues of the circulant matrix \mathbf{Z} . The pre- and post-multiplication of Γ_Z respectively by the diagonal matrices Γ_{2N}^\dagger and Γ_{2N} yields $\Gamma_{2N}^\dagger \Gamma_Z \Gamma_{2N}$, which, as the three matrices are diagonal, becomes $\Gamma_{2N}^\dagger \Gamma_{2N} \Gamma_Z = \Gamma_Z$. We then rewrite (20) as

$$\begin{aligned} \Phi_{2N} \mathbf{Z} \Phi_{2N}^\dagger &= \mathbf{F}_{2N}^\dagger \Gamma_Z \mathbf{F}_{2N} \\ &= \mathbf{F}_{2N}^\dagger (\mathbf{F}_{2N} \mathbf{Z} \mathbf{F}_{2N}^\dagger) \mathbf{F}_{2N} \\ &= \mathbf{Z}, \end{aligned} \quad (21)$$

which proves (18).

Convolution theorem of the modified DFNT

Considering two vectors $\mathbf{a} \in \mathbb{R}^{2N \times 1}$ and $\mathbf{b} \in \mathbb{R}^{2N \times 1}$, to which are associated the circulant matrices $\mathbf{A} \in \mathbb{R}^{2N \times 2N}$ and $\mathbf{B} \in \mathbb{R}^{2N \times 2N}$, respectively, one can write the circular convolution between \mathbf{a} and \mathbf{b} as

$$\mathbf{c} = \mathbf{A} \mathbf{b} \quad (22)$$

$$= \mathbf{B} \mathbf{a}, \quad (23)$$

where $\mathbf{c} \in \mathbb{R}^{2N \times 1}$. By applying the DFNT on \mathbf{c} , one obtains its discrete Fresnel domain representation $\dot{\mathbf{c}} \in \mathbb{R}^{2N \times 1} = \Phi_{2N} \mathbf{c}$, which can be rewritten as

$$\dot{\mathbf{c}} = \Phi_{2N} \mathbf{A} \mathbf{b} \quad (24)$$

$$= \Phi_{2N} \mathbf{B} \mathbf{a}. \quad (25)$$

Making use of the unitary and similarity transformation properties of the DFNT from (17) and (18), respectively, (24) and (25) can be further rearranged respectively as

$$\dot{\mathbf{c}} = \Phi_{2N} \mathbf{A} \Phi_{2N}^\dagger \Phi_{2N} \mathbf{b} \quad (26)$$

$$= \Phi_{2N} \mathbf{B} \Phi_{2N}^\dagger \Phi_{2N} \mathbf{a}. \quad (27)$$

Using the similarity transformation property from (18), it is known that $\Phi_{2N} \mathbf{A} \Phi_{2N}^\dagger = \mathbf{A}$ and $\Phi_{2N} \mathbf{B} \Phi_{2N}^\dagger = \mathbf{B}$. Hence, (26) and (27) become respectively

$$\dot{\mathbf{c}} = \mathbf{A} \Phi_{2N} \mathbf{b} \quad (28)$$

$$= \mathbf{B} \Phi_{2N} \mathbf{a}, \quad (29)$$

in which $\dot{\mathbf{a}} = \Phi_{2N} \mathbf{a}$ and $\dot{\mathbf{b}} = \Phi_{2N} \mathbf{b}$ are the Fresnel domain representations of \mathbf{a} and \mathbf{b} , respectively.

From (28) and (29), it is seen that the DFNT of the circular convolution between \mathbf{a} and \mathbf{b} can be interpreted as the circular convolution between \mathbf{a} and $\dot{\mathbf{b}}$ or, alternatively, as the circular convolution between \mathbf{b} and $\dot{\mathbf{a}}$.

REFERENCES

- [1] M. Sedighizadeh, A. Rezaadeh, and N. I. Elkalashy, "Approaches in high impedance fault detection - a chronological review," *Advances in Electrical and Computer Engineering*, vol. 10, no. 3, pp. 114–128, Aug 2010.
- [2] A. Ghaderi, H. L. Ginn, and H. A. Mohammadpour, "High impedance fault detection: A review," *Electric Power Systems Research*, vol. 143, pp. 376 – 388, Feb. 2017.
- [3] F. Auzanneau, "Wire troubleshooting and diagnosis: Review and perspectives," *Progress In Electromagnetics Research B*, vol. 49, pp. 253–279, 2013.
- [4] A. N. Milioudis, G. T. Andreou, and D. P. Labridis, "Detection and location of high impedance faults in multiconductor overhead distribution lines using power line communication devices," *IEEE Transactions on Smart Grid*, vol. 6, no. 2, pp. 894–902, March 2015.
- [5] F. Passerini and A. M. Tonello, "Smart grid monitoring using power line modems: Anomaly detection and localization," *Cornell University Library*, pp. 1–8, July 2018. [Online]. Available: <https://arxiv.org/abs/1807.05347>
- [6] Y. Huo, G. Prasad, L. Lampe, and V. C. M. Leung, "Cable diagnostics with power line modems for smart grid monitoring," *Cornell University Library*, pp. 1–8, Aug. 2018. [Online]. Available: <https://arxiv.org/abs/1808.01149>
- [7] L. G. de Oliveira, M. de L. Filomeno, L. F. Colla, H. V. Poor, and M. V. Ribeiro, "On the suitability of PLC pulses for power line fault sensing via time-domain reflectometry," *Cornell University Library*, pp. 1–13, Jan. 2019. [Online]. Available: <https://arxiv.org/abs/1901.07923>
- [8] F. Auzanneau, "Transferometry: A new tool for complex wired networks diagnosis," *Progress In Electromagnetics Research B*, vol. 70, pp. 87–100, 2016.
- [9] S. Naik, C. M. Furse, and B. Farhang-Boroujeny, "Multicarrier reflectometry," *IEEE Sensors Journal*, vol. 6, no. 3, pp. 812–818, June 2006.
- [10] P. Amini, C. Furse, and B. Farhang-Boroujeny, "Filterbank multicarrier reflectometry for cognitive live wire testing," *IEEE Sensors Journal*, vol. 9, no. 12, pp. 1831–1837, Dec. 2009.
- [11] A. Lelong and M. O. Carrion, "On line wire diagnosis using multicarrier time domain reflectometry for fault location," in *Proc. IEEE SENSORS*, Oct. 2009, pp. 751–754.
- [12] W. B. Hassen, F. Auzanneau, L. Incarbonne, F. Pérès, and A. P. Tchangan, "Distributed sensor fusion for wire fault location using sensor clustering strategy," *International Journal of Distributed Sensor Networks*, vol. 11, no. 4, pp. 1–17, April 2015.
- [13] L. G. de Oliveira, M. de L. Filomeno, and M. V. Ribeiro, "HS-OFDM-based time-domain reflectometry for power line sensing: Characteristics and limitations," *Cornell University Library*, pp. 1–12, Jan. 2019. [Online]. Available: <https://arxiv.org/abs/1901.08404>
- [14] A. Lelong, L. Sommervogel, N. Ravot, and M. O. Carrion, "Distributed reflectometry method for wire fault location using selective average," *IEEE Sensors Journal*, vol. 10, no. 2, pp. 300–310, Feb. 2010.
- [15] X. Ouyang and J. Zhao, "Orthogonal chirp division multiplexing," *IEEE Transactions on Communications*, vol. 64, no. 9, pp. 3946–3957, Sep. 2016.
- [16] L. de M. B. A. Dib, "Multichirp code division multiple access for smart grids and internet of things," Master's thesis, Federal University of Juiz de Fora, Brazil, 2018.
- [17] S. K. Mitra, *Digital Signal Processing: A Computer-Based Approach, 4th Edition*. McGraw-Hill, 2010.
- [18] X. Ouyang, O. A. Dobre, and J. Zhao, "Unbiased channel estimation based on the discrete fresnel transform for CO-OFDM systems," *IEEE Photonics Technology Letters*, vol. 29, no. 8, pp. 691–694, April 2017.
- [19] X. Ouyang, C. Antony, G. Talli, and P. D. Townsend, "Robust channel estimation for coherent optical orthogonal chirp-division multiplexing with pulse compression and noise rejection," *Journal of Lightwave Technology*, vol. 36, no. 23, pp. 5600–5610, Dec. 2018.
- [20] L. Lampe and A. J. H. Vinck, "On cooperative coding for narrow band PLC networks," *AEU - International Journal of Electronics and Communications*, vol. 65, no. 8, pp. 681–687, Aug. 2011.
- [21] "IEEE standard for low-frequency (less than 500 kHz) narrowband power line communications for smart grid applications," *IEEE Std 1901.2-2013*, pp. 1–269, Dec. 2013.
- [22] C. R. Paul, *Analysis of Multiconductor Transmission Lines, 2nd Edition*. John Wiley & Sons Inc., 2007.
- [23] L. Lampe, A. M. Tonello, and T. G. Swart, *Power Line Communications: Principles, Standards and Applications from Multimedia to Smart Grid, 2nd Edition*. John Wiley & Sons Inc., 2016.
- [24] L. Franek and P. Fiedler, "A multiconductor model of power line communication in medium-voltage lines," *Energies*, vol. 10, no. 6, pp. 1–16, 2017.
- [25] Z. Tao, Y. Xiaoxian, Z. Baohui, N. H. Xu, F. Xiaoqun, and L. Changxin, "Statistical analysis and modeling of noise on 10-kv medium-voltage power lines," *IEEE Transactions on Power Delivery*, vol. 22, no. 3, pp. 1433–1439, July 2007.
- [26] M. Giroto and A. M. Tonello, "EMC regulations and spectral constraints for multicarrier modulation in PLC," *IEEE Access*, vol. 5, pp. 4954–4966, Mar. 2017.